Separation and Purification Technology 361 (2025) 131093

Contents lists available at ScienceDirect

Separation and Purification Technology

journal homepage: www.elsevier.com/locate/seppur

Experimental and theoretical investigation of the pressure drop across different surface filter media at low absolute pressures down to 100 Pa

Vanessa Löschner *, Jörg Meyer, Achim Dittler

KIT, Institute of Mechanical Process Engineering and Mechanics (MVM) – Research Group Gas Particle Systems, Straße am Forum 8, 76131, Karlsruhe, Germany

ARTICLE INFO

Communicated by Volodymyr Tarabara

Keywords:
Surface filtration
Pressure drop
Calculation model
Low pressure applications

ABSTRACT

Some gas particle separation processes operate under low absolute pressures. Surface filter media are typically used in these applications. Little is known about the pressure drop behavior of surface filters under low pressure conditions. It is essential to obtain a more profound comprehension of filtration processes at low absolute pressures, in order to ensure the optimal sizing of the filtration system. An important factor in the layout of surface filters is the pressure drop across the filter media. In this study, the pressure drop was measured for five types of surface filter media at three filter face velocities, as a function of absolute pressure at ambient temperature in air. The absolute pressure was varied from 100 to 10^5 Pa. It has been shown that the pressure drop across the surface filter media decreases when the absolute pressure is reduced. The measured pressure drop values of all filter media demonstrated a qualitatively analogous trend at all three velocities. Additionally, a semi-empirical model for the calculation of the pressure drop across pipes was applied. This model enables the determination of the pressure drop across surface filter media under low pressure conditions. The calculated pressure drop values demonstrate a high degree of agreement with the measured values (max. deviation of 20% down to 5000 Pa, for lower absolute pressures the deviations become higher). It is possible to calculate the pressure drop within this range using a single pressure drop measurement conducted under ambient conditions, along with the known filter face velocity, temperature, filter media- and fluid-specific parameters.

1. Introduction

The importance of process-integrated particle separation in many industrial applications is well documented in the literature [1–5]. One area of application with advanced requirements for corresponding filter systems are vacuum drying processes due to the low process pressure. There, low process pressures are necessary to ensure high drying rates while protecting the typically temperature-sensitive bulk materials, such as fine chemicals or pharmaceuticals, from overheating and subsequent thermal decomposition of the active ingredient [6,7]. For products that require a very low residual moisture, absolute pressures down to 100 Pa are needed [6]. During vacuum drying, liquid from the drying bulk is vaporized. The rising vapor can entrain fine particles from the bulk material into the gas flow [8]. To prevent contamination of the downstream system components, for example the pump system and the condenser, the rising vapor stream laden with particles has to be filtered [6–8]. In this field of application, the filters are called vapor filters. In the majority of cases, surface filter media are employed in vacuum drying processes, given that vapor flow rates and resulting filter face velocities are typically low. Continuous operation of the cleanable filter media as well as high separation efficiencies and recovery of collected product through inline regeneration are additional process benefits [8–10].

The current layout of surface filters for vacuum drying processes is often based on data obtained under ambient pressure conditions and inert gases (no vapor/condensable gaseous components). However, this often leads to inadequate dimensioned filter systems for the vacuum drying application. It is observed that filter areas which are too small result in an accelerated accumulation of dust, leading to a correspondingly rapid rise in pressure drop. The use of pressure drop-controlled cleaning may result in the occurrence of unstable filter operation and an increase in energy consumption due to the necessity for more frequent regeneration. Moreover, it can result in greater compaction of the filter cake, which increases the adhesive forces and consequently can lead to incomplete regeneration. Furthermore, each jet-pulsed regeneration of the filter medium results in the generation of short-term pressure peaks, which not only increase the pressure within the filter element itself but also throughout the entirety of the drying chamber. Consequently, the saturation rises abruptly in the majority of the filter volume, with the vapor condensing on the solid particles and the filter media. This causes the particle material to adhere and cake on the filter, resulting in an

* Corresponding author.
E-mail address: vanessa.loeschner@kit.edu (V. Löschner).

https://doi.org/10.1016/j.seppur.2024.131093
Received 20 October 2024; Received in revised form 13 December 2024; Accepted 13 December 2024
Available online 25 December 2024

Table 1
Classification of the different flow regimes using the Kn-number.

Continuum flow:	0 < Kn < 0.001
Slip flow:	0.001 < Kn < 0.25
Transitions flow:	0.25 < Kn < 10
Molecular flow:	10 < Kn

increase in absolute pressure on the filter. Furthermore, the irreversible accumulation of dust in the filter medium leads to a change in media flexibility and strength, which results in deformation or damage to the filter elements. The only solution here is to replace or externally clean the filter elements, which requires plant shutdown and production downtime.

The use of excessively large filter areas on the other hand has economic drawbacks. In order to enhance the existing dimensioning guidelines, it is essential to gain a fundamental understanding of the operational characteristics (pressure drop with and without dust loading, cake built-up processes, separation efficiencies etc.) of surface filters at low pressures. An important parameter for filter area dimensioning is the pressure drop across the unladen filter medium for a certain filter face velocity [11].

The governing parameter for describing the flow conditions at different absolute pressures is the Knudsen number (Kn-number). It is defined as the ratio of the mean free path of the gas molecules λ to a characteristic linear dimension of the flow path (Eq. (1)) [12–14].

$$Kn = \frac{\lambda}{a} \tag{1}$$

The mean free path of the gas molecules λ specifies how much of a path a gas molecule can travel on average until it collides with another gas molecule. The mean free path of the gas molecules λ can be calculated using Eq. (2) [15,16]:

$$\lambda = \frac{k_B \cdot T}{\sqrt{2} \cdot \pi \cdot d^2 \cdot p} \tag{2}$$

The mean free path of the gas molecules λ depends on the Boltzmann constant k_B, the temperature T, the molecular diameter of the fluid d and the absolute pressure p. The Kn-number can thus be varied by the temperature, the pore diameter (or fiber radius and porosity of a fibrous filter medium) and the absolute pressure. The mean fiber radius or the mean pore diameter can be used as the characteristic length for calculating the Kn-number [12,13]. In this work, the mean pore diameter of the filter media is used as the characteristic length for determining the Kn-number. A number of different ranges of the Kn-number have already been defined in the literature. In this work, the authors use the definition in Table 1 for the corresponding flow regimes [11,12,17,18]:

Fig. 1 shows a schematic illustration of the Kn-number as a function of the absolute pressure for three different mean pore diameters at a constant temperature of 20 °C. The continuum regime is only just being reached at an average pore diameter of 100 µm under nearly ambient conditions. The Kn-number increases with a reduction in the mean pore diameters at a constant absolute pressure.

In the continuum regime, the fluid is considered as a continuum. The interactions between the molecules predominate over those between molecules and walls. Transitioning into the slip flow regime, the 'no slip' condition of the flow at the wall no longer applies. As the Kn-number increases, the mean free path of the gas molecules takes on dimensions similar to the characteristic length of the flow path. If the mean free path is the dominating factor compared to the characteristic length, a molecular flow is present [13,16].

It is known from the literature for studies of depth filters at various absolute pressures that the pressure drop decreases with lower absolute pressure (except in the continuum regime where the pressure drop is

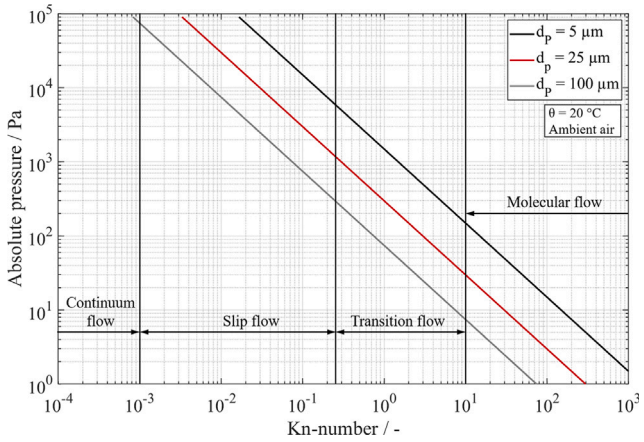

Fig. 1. Schematic representation of the Knudsen number as a function of absolute pressure for three different mean pore diameters at a constant temperature of 20 °C.

constant with regard to the absolute pressure). Thus, the pressure drop decreases as the Kn-number increases [12,19–23]. Through the use of carbon nanotubes as filter material it is possible to reach the free molecular flow regime at ambient conditions [11]. Although available for various depth filter media since decades, no measurements of pressure drops for surface filters at low pressures were found in the available literature.

The most common basis for various calculations of the pressure drop across fibrous filter media is provided by Fuchs et al. [24]. This approach is based on the one hand on the Kuwabara model (disordered, homogeneous structure of parallel cylinders perpendicular to the direction of flow [25]) and on the other hand on the resistance theory of porous materials [26]. Many different authors report calculation models for the pressure drop of fibrous filters dependent on the corresponding flow regime [18,19,27–30]. According to Davies et al. these calculation methods provide good correlations with the experimental data [12].

Surface filter media can (and will) have different properties (Table 2), especially due to the much higher solid fraction and the elaborate surface treatment to promote particle separation on the surface of the filter material. This puts the existing calculation models into question, as their validity was demonstrated using highly porous depth filter. In a series of experiments performed by the authors, the pressure drop of different surface filter media was investigated in ambient air at low absolute pressure levels at ambient temperature. Applying the established equations reported in literature did not sufficiently reflect the actual behavior observed in the experiments. This is attributed by the authors to the porosity level of the used filter media, as these have a significantly lower porosity compared to depth filters. Therefore, the assumptions made when calculating the pressure drop as they apply to depth filters (like Kuwabara model [25]) are no longer valid for surface filters [12,19]. No calculation equations explicitly developed for the pressure drop at low pressures for surface filters have yet been found in the literature, so the authors have applied and adapted a model for micro- and nano flows through pipes, ducts and channels presented in Section 2 [14,31,32].

This paper focuses on the comparison between calculated and measured pressure drops across five surface filter media with different and complex structures without particle loading at low absolute operating pressures down to 100 Pa at ambient temperature and in ambient air.

2. Calculation model for pressure drop across surface filter media based on equations proposed by Beskok et al. [14]

The structure of surface filter media are highly complex, comprising a variety of elements such as non-woven sintered or non-sintered layers

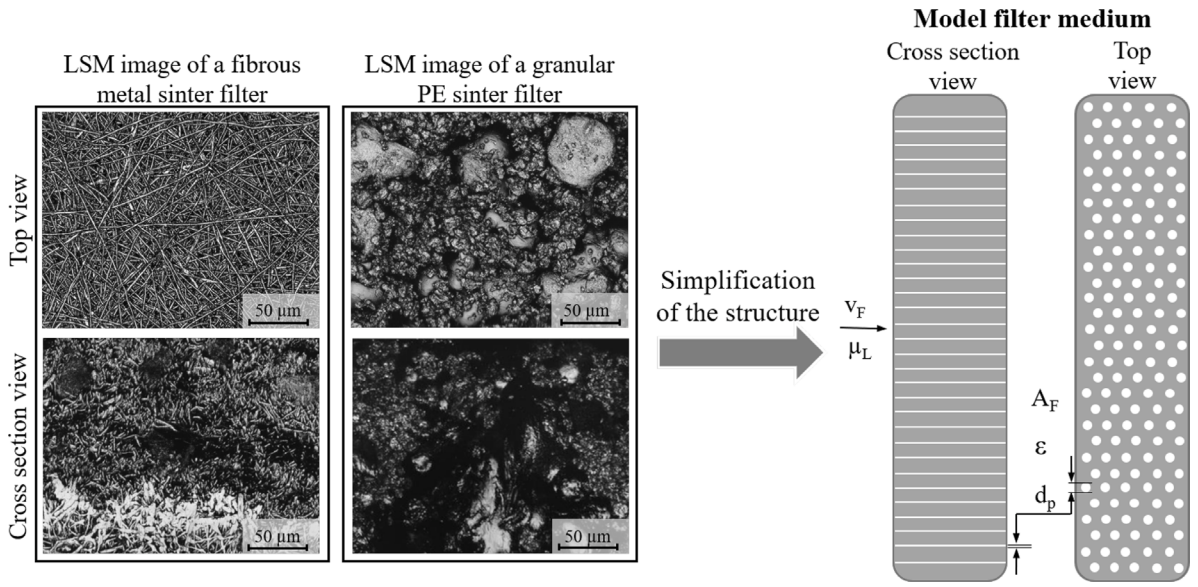

Fig. 2. Model simplifications for calculating the pressure drop of surface filter media at low absolute pressures.

of fibers, woven meshes, or sintered granules. Surface filter media are often composed of multiple layers [17]. For example, high performance media consist of a needle felt medium as a carrier with an additional fine fiber layer or e-PTFE membrane lamination, or sintered granular PE filters as a carrier with a fine sintered PPS coating. Furthermore, surface filter media frequently exhibit a highly inhomogeneous structure. The pressure drop characterization of such filter media is therefore a complex undertaking, necessitating the development of a simplified calculation model for mathematical description. One potential simplification of the filter medium structure is illustrated in Fig. 2. In this model, the filter medium is simplified as a row of parallel, straight pipes with an average diameter d_P. Here d_P is an appropriate flow-related equivalent diameter rather than a simple geometric dimension of the filter structure.

It is further assumed that a micro or nano flow is present in the pipes of the filter medium. Beskok et al. provide a universal equation for calculating the pressure distribution as a function of the position along a pipe for the entire Kn-number regime (Eq. (3)) [31]:

$$\dot{V} = \underbrace{\frac{-\pi\left(\frac{d_P}{2}\right)^4}{8\mu}\cdot\frac{dp}{dx}}_{I}\cdot\underbrace{\left(1+\frac{4Kn}{1-bKn}\right)}_{II}\cdot\underbrace{C_r}_{III} \tag{3}$$

Where $\dot{V}$ is the flow rate in the filter medium, d_p is here the mean pore diameter of the filter medium, μ is the dynamic gas viscosity, Kn is the Kn-number, b is the slip coefficient and C_r is the rarefaction coefficient. The flow rate is defined as:

$$\dot{V} = \frac{v_F\pi\left(\frac{d_p}{2}\right)^2}{\varepsilon} \tag{4}$$

where v_F is the filter face velocity and ε the mean porosity of the filter medium.

Eq. (3) is made up of three parts. The first part (I) describes the volume flow through a pipe in the continuum regime. The second part of Eq. (3) (II) corrects the volume flow due to slip effects with increasing Knudsen number, as the velocity at the pipe wall no longer corresponds to zero from the slip flow range. The third part of Eq. (3) (III) corrects the volume flow due to rarefaction effects.

For the correction of the volume flow due to the slip effect, Beskok et al. assumed a two-dimensional isothermal flow. DSMC (Direct Simulation Monte-Carlo) simulations and the solution of the linearized Boltzmann equation have shown that the parabolic flow shape and wide ranges of the Kn-number are maintained. For this reason, Beskok et al. assumed a parabolic flow profile with a consistent slip condition over the entire range of the Kn-number [32]. The slip boundary condition (Eq. (5)) derived by Beskok et al. corresponds to a second order boundary condition and is valid in the entire Kn-number range and for compressible flows:

$$U_s - U_x = \frac{2-\sigma_v}{\sigma_v}\cdot\left[\frac{Kn}{1-bKn}\left(\frac{\partial U}{\partial n}\right)_s\right] \tag{5}$$

U corresponds to the non-dimensional velocity (non-dimensionalization with a reference velocity), σ_v to the tangential accommodation coefficient (tangential momentum exchange of gas molecules with surfaces), n denotes the outward normal vector and b is the general slip coefficient.

The tangential momentum accommodation coefficient σ_v can be defined in two limiting cases:

- $\sigma_v = 0$ specular reflection: The tangential velocity of the molecules that are reflected by the walls remains constant. The velocity of the reflected molecules is reversed due to the transfer of normal momentum to the wall. In this case, there is no tangential momentum exchange between the fluid and the wall, which results in zero skin friction. [31]
- $\sigma_v = 1$ diffuse reflection: the molecules are reflected with an average tangential velocity of zero. There is a tangential momentum exchange between the wall and the molecules, which leads to friction. [31]

From the solution of the linearized Boltzmann equation and the use of DSMC simulations, a value of b = −1 can be applied for b in the entire Kn-number range. In addition, b is independent of the used gas (Air, He, N).

The rarefaction factor, designated as Cr in Eq. (3), is introduced to describe the influence of rarefaction with decreasing absolute pressure on the volume flow. According to Beskok et al. the following equation can be used in the entire Kn-number range:

$$Cr = (1+\alpha Kn) \tag{6}$$

Where α is an empirical correction factor [14]. The rarefaction coefficient incorporates the decrease in intermolecular collisions with increasing Kn-number. It therefore reflects the ratio between the number of intermolecular collisions and the number of all collisions (intermolecular collisions and collisions of molecules with the wall). The

factor α itself is a function of the Kn-number and thus of the absolute pressure. For very large Kn-numbers (free-molecular range), α approaches a constant value. For small Kn-numbers, however, α must tend towards zero, as rarefaction effects no longer play a role at ambient pressures [31].

To calculate the pressure drop, it is necessary to calculate the integral of Eq. (3), setting the thickness of the filter medium and the inlet pressure (p_i) and the outlet pressure (p_o) as integration limits. Integration of Eq. (3) and substituting Eq. (1) and (2) into Eq. (3) yields Eq. (7).

$$L = C_1 \cdot \left[\frac{4C_2 b + 4C_2\alpha \cdot \ln(p_o - C_2 b) + (C_2\alpha b - 4C_2\alpha) \cdot \ln(p_o) + b(p_o)}{b} - \frac{4C_2 b + 4C_2\alpha \cdot \ln(p_i - C_2 b) + (C_2\alpha b - 4C_2\alpha) \cdot \ln(p_i) + b(p_i)}{b} \right] \tag{7}$$

p_o is the absolute pressure downstream of the filter medium, p_i is the absolute pressure upstream of the filter medium and L is the thickness of the filter medium. C_1 and C_2 are filter material- and fluid-specific constants and are defined as follows in Eqs. (8) and (9):

$$C_1 = \frac{-\pi \left(\frac{d_p}{2}\right)^4}{8\mu \dot{V}} \tag{8}$$

$$C_2 = \frac{k_B T}{\sqrt{2}\pi d^2 d_p} \tag{9}$$

where d_p is the mean pore diameter of the filter medium, μ is the dynamic viscosity, k_B is the Boltzmann-constant, T is the temperature and d is the mean molecule diameter of the fluid. An ideal gas is assumed for ambient air, therefore the viscosity can be considered as constant. p_o and p_i can be obtained during measurements. The empirical correction factor α can consequently be determined iteratively by solving Eq. (7) numerically, for various α values. α is a function of the Kn number and the absolute pressure for a specific geometry (here for a specific filter medium). It is thus necessary to determine a fit function for α = f(Kn or p) for each filter medium. For simple geometries such as long straight pipes with a constant cross-section, equations for the fit of α are available in the literature [31]. However, these are no longer valid for the complex 'pipe structure' in a filter medium due to tortuosity, cross-connections, changes in cross-section, and other factors. Finally Section 4.3 presents two different methods to determining a modified media-specific fit function for α based on a small number of pressure drop measurements in ambient air and at ambient temperature. The determined α can be used to calculate the pressure p_o downstream of the filter medium. The difference between p_o and p_i yields the desired pressure drop across the filter medium. For a more precise calculation of the pressure drop, a pore size distribution or a porosity distribution for the filter media can be determined instead of an average pore size or porosity. Nevertheless, such measurements are time-consuming, and thus the average values for the pore diameter and porosity are employed in this study.

3. Material and methods

3.1. Experimental setup

3.1.1. Volume flow and absolute pressure adjustment

A schematic of the experimental setup used for all tests in this study is shown in Fig. 3.

Ambient air (neglecting of humidity and fine particles in the ambient air) is drawn in by a compressor, which serves to regulate the volume flow within the filter chamber and, consequently, the filter face velocity. The incoming volume flow is pre-throttled in a first step by a critical nozzle. Different diameters of the critical nozzles (CN) are selected for different combinations of volume flow and absolute pressure in the filter chamber ($d_{CN,1}$ = 1.36 mm and $d_{CN,2}$ = 2.94 mm). Afterwards, the volume flow is precisely adjusted with the help of a pinch valve (from KVT GmbH, with a nominal diameter (outside diameter) of the hose to be compressed of 6 (DN 6)). The flow rate is measured downstream of the compressor at ambient conditions (p_{abs} = 10^5 Pa, θ = 20 °C) using a mass flow meter (MFM). Two thermal MFMs from MKS Instruments Deutschland GmbH were used to completely cover the volume flow range to be measured (Full scale range of 2 L min^{-1} and 50 L min^{-1} with a resolution of 0.1 % of full scale). The volume flow is adjusted so that the filter face velocity remains constant at different absolute pressures.

With the help of a butterfly valve (from VAT Group AG, with a ISO KF DN 25 flange type) and a gas control valve (EVR 116 from Pfeiffer Vacuum GmbH, with a ISO KF DN 16 flange type and a control range from 5×10^{-6} Pa L min^{-1} to 1250 mbar L min^{-1}) after the filter chamber, the absolute pressure on the raw gas side in the filter chamber is regulated. The gas control valve is employed for the purpose of manually establishing a specific gas flow value. The pressure is precisely regulated by use of the butterfly valve. Due to the critical nozzle at the inlet, it is possible to adjust the volume flow and absolute pressure independently of each other. Three different filter face velocities v_F (2 cm s^{-1}, 5 cm s^{-1} and 10 cm s^{-1}) and a pressure range of p_{abs} = 100 – 10^5 mbar were investigated.

3.1.2. Filter chamber

The center of the experimental setup is the filter chamber, a picture is shown in Fig. 4. The filter chamber has a length of 152 cm and a diameter of 19 cm. After an inlet distance of 53 cm, the filter holder including the filter medium is installed. The filter holder can be equipped with spacer rings, making it possible to clamp filter media of varying thicknesses. The effective free flow area of the filter medium is 0.0154 m^2. In the filter chamber the temperature (Temperature sensor Pt 100 4-wire) and the absolute pressure (vacuum transmitter pirani from Thyracont Vacuum Instruments GmbH, with a absolute pressure measuring range from 5×10^{-5} mbar to 2000 mbar and a precision of < 2 % for p_{abs} = 2000 – 200 mbar, < 5 % for p_{abs} = 200 – 40 mbar and < 10 % for p_{abs} = 40 – 2×10^{-3} mbar) were measured at the raw gas side. Additionally the pressure drop across the filter medium is measured with a differential pressure transmitter (from ICS Schneider Messtechnik GmbH, with a measuring range up to 50 mbar and a resolution of ±0.2 % of full scale). The absolute pressure on the clean gas side of the filter medium can be monitored with a handheld pressure gauge.

3.2. Selected filter media

In this study, five different surface filter media were tested:

- Needle felt medium with broad hydro-entangled polyethersulfon (PES) fibers (NF)
- Woven metal fiber medium (WMF)
- Non-woven sintered metal fiber medium (SMF)
- Sintered granular PE (Polyethylene) medium (SG)
- The same sintered PE (Polyethylene) medium with a sintered PPS (Polyphenylene sulfide) coating (SGC)

Laser scanning microscope (LSM) images of the various filter media are shown in Fig. 5. These images show the structural variations between the different media.

An overview of the most important properties of the filter media is shown in Table 2.

The mean pore sizes were determined by porometry, except for the woven metal filter medium, where the mean pore diameter is equivalent to the geometric pore size (corresponds to the diameter of a spherical particle that can just pass through the mesh). If there was no information on porosity available in the manufactures data sheet, a corresponding porosity value was calculated using Eq. (10):

$$\varepsilon = 1 - \frac{W}{\rho L} \tag{10}$$

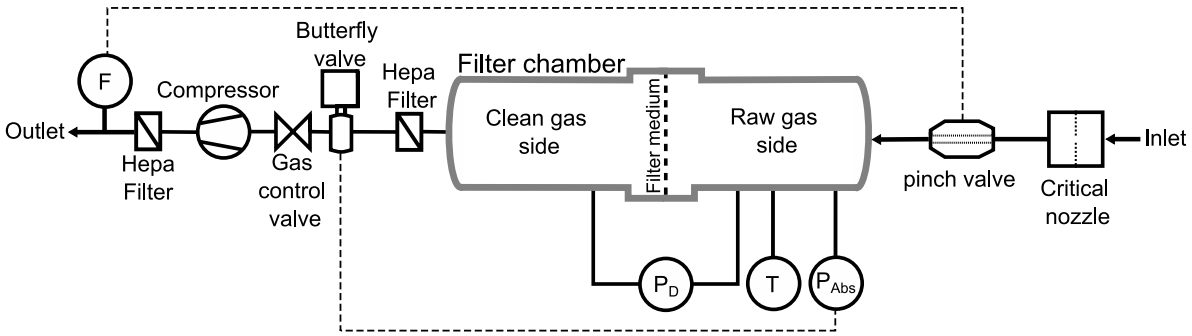

Fig. 3. Schematic illustration of the experimental setup.

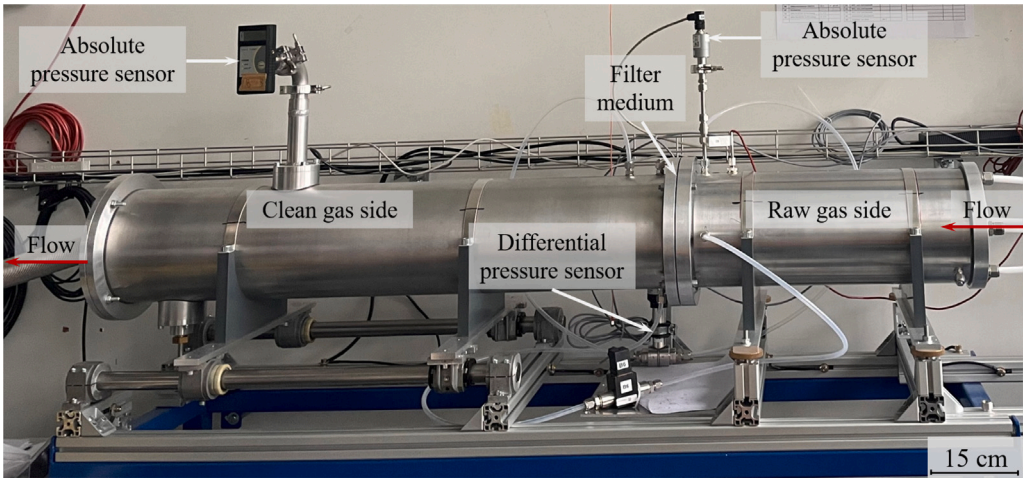

Fig. 4. Picture of the filter chamber.

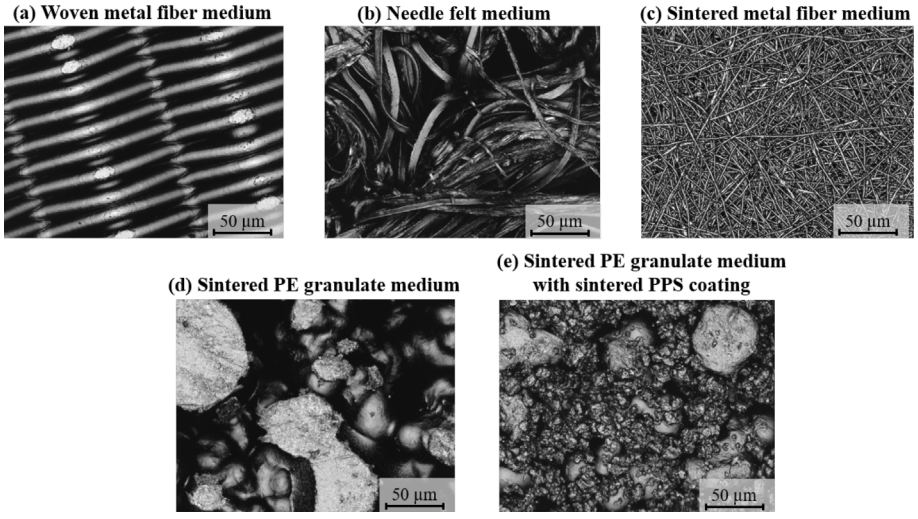

Fig. 5. Laser scanning microscope (LSM) top view images of five different surface filter media used in this work. (a) Woven metal fiber medium (b) Needle felt medium (c) Sintered metal fiber medium (d) Sintered PE granulate medium (e) Sintered PE granulate medium with sintered PPS Coating.

where ε is the mean porosity, W the basis weight (mass per filter area), ρ the density of the fibers or granules and L the thickness of the filter medium. The selected filter media cover a large range of mean pore diameters starting from 1.36 µm for the sintered metal fiber medium to 28.6 µm for the sintered granular PE medium without coating. In addition, their porosities are typical for surface filter media and hence much smaller than $\varepsilon \approx 1$. The thickness/pore diameter (length/pore diameter) ratio of the filter media is also shown in Table 2. All filter media have high thickness/pore diameter ratios in a range from 14 for the woven metal fiber medium to a value of 331 for the sintered metal fiber medium. For the sintered granular PE medium with the sintered PPS coating, it is important to mention that the specification of the mean pore size refers to the coating. The coating is responsible for the main pressure drop for determination of the mean pore size using porometry. However, the thickness of this filter medium refers to the total thickness of the medium, consisting of support structure and

Table 2
Properties of the selected filter media.

Filter medium	Label	Mean pore size d_p/ µm	Mean fiber diameter d_f/ µm	Mean porosity ε	Basis weight W/g m^{-2}	Thickness L/mm	L/d_p
Needle felt medium	NF	14.35[a]	13.64[f]	0.82[b]	240	1	70
Woven metal medium	WMF	5[e]	14[f]	0.68	230	0.07	14
Sintered metal fiber medium	SMF	1.36[a]	1[f]	–	1200	0.45	331
Sintered granular PE medium without sintered PPS Coating	SG	28.6[a]	–	0.47[b]	2066	4	140
Sintered granular PE medium with sintered PPS Coating	SGC	4.82[a]	–	0.46[b]	2148	4[c]	830

[a] Determined by porometry.
[b] Determined with Eq. (10).
[c] Total thickness (substrate structure + coating).
[e] Geometric pore size.
[f] Determined from the LSM images.

(d) Refers to the lamination layer.

coating (coating thickness not specified by manufactures data sheet).

4. Results and discussion

4.1. Characterization of the flow conditions through the filter medium

In order to characterize the existing flow conditions at different absolute pressures, a variety of non-dimensional parameters can be utilized, taking into account the specific characteristics of the flow, such as whether it is laminar or turbulent (Re-number), compressible or incompressible (Ma-number), and whether or not a slip effect is present (Kn-number).

Table 3 shows these non-dimensional numbers for the characterization of the flow through various filter media at ambient temperature in air for a filter face velocity of 10 cm s^{-1}. This is the highest filter face velocity that has been subject to this investigation. Turbulence or compressibility effects are absent at this filter face velocity, it can be assumed that these phenomena can also be neglected at lower filter face velocities. The Kn-number (Eq. (1)), Re-number (Eq. (11)), and Ma-number (Eq. (12)) were calculated on the upstream (filter medium inlet, indices i) and downstream side (filter medium outlet, indices o) of the different filter media at p = 10^5 Pa and p = 100 Pa at a filter face velocity of 10 cm s^{-1} with the following equations for Re and Ma:

$$Re = \frac{\rho v_F d_p}{\mu} \tag{11}$$

$$Ma = \frac{v_f}{c} \tag{12}$$

Where ρ is the density of the fluid, v_F is the filter face velocity, d_p the mean pore diameter of the filter medium, μ is the dynamic viscosity of the fluid and c is the speed of sound.

The Kn-number varies from the slip flow regime to free molecular flow. None of the filter media reached the continuum regime even at ambient absolute pressures. It can be stated that the slip effect is present for all filter media. The Re-number for all measured pressure ranges and filter media is always much smaller than 1 ($Re \ll 1$). The flow within the filter medium can therefore be assumed to be laminar for all testing conditions. The Ma-number is much smaller than $Ma \approx 0.3$ for all filter media used and all filter face velocities, so the flow through the different filter media can be considered non-compressible in the entire investigated absolute pressure range [31].

4.2. Pressure drop measurement of different surface filter media at low absolute pressures for different filter face velocities

The objective of this study was to investigate the pressure drop (Δp) of five distinct filter media at three different filter face velocities, namely 2 cm s^{-1}, 5 cm s^{-1} and 10 cm s^{-1}, within a pressure range of p_{abs} = 100 – 10^5 Pa in air at ambient temperature. The results of the pressure drop measurements as a function of the absolute pressure are presented in Fig. 6.

The pressure drop curve for each constant filter face velocity is shown. The triangles represent the pressure drop values, and the dashed lines represent connecting lines between them. All measurements were carried out three times, using the same filter medium sample (to exclude possible influences due to inhomogeneities between different filter medium samples). For the lowest filter face velocity of 2 cm s^{-1}, tests were only carried out for the sintered metal fiber medium and both sintered PE granulate media. The other filter media (NF and WMF) showed very small pressure drops even at higher filter face velocities. With the applied measurement equipment, the smallest pressure drops cannot be measured accurately at low absolute pressures (p_{abs} < 500 Pa). For the WMF medium, negative pressures drops were measured at 10 cm s^{-1} and 5 cm s^{-1}, and for the NF medium at 5 cm s^{-1}, again due to the resolution limit of the differential pressure sensor. For this reason, the respective values in Fig. 6 are omitted.

All measured pressure drop curves plotted as a function of the absolute pressure for the different filter media show the same qualitative trend for all tested filter face velocities. The pressure drop across the surface filters decreases with the reduction in absolute pressure for all filter media. This behavior is consistent with that observed in depth filter media in previously cited literature [12,17,20,21]. The reduction in pressure drop with decreasing pressure can be attributed to the rarefaction of the system and the associated increase in the mean free path of the gas molecules. Higher rarefaction leads to lower frictional energy losses of the gas flow based on fewer collisions between gas molecules and collector surfaces (e.g. fibers) of the filter medium as well as the increasing relevance of the slip effect.

Additionally, it can be seen that the slope of the pressure drop curves $\left(\frac{d\log\Delta p}{d p_{abs}}\right)$ is nearly flat at high absolute pressures, near 10^5 Pa, for all filter face velocities. The slope in this range is almost 0 for the filter medium with the largest mean pore diameter (SG) and is steepest for the filter medium with the smallest mean pore diameter (SMF). As the absolute pressure decreases, the pressure drop slope $\left(\frac{d\log\Delta p}{d p_{abs}}\right)$ increases and appears to become constant towards the lower end of the investigated absolute pressure range.

The various filter media vary widely in their structural properties (d_p, L, ε), which affects the resulting pressure drop across the filter medium. To compare the pressure drop of the different filter media, Table 4 lists the pressure drop at ambient conditions for all three filter face velocities in air. At this absolute pressure the Kn-numbers are lowest and thus, the flow through the filter media is close to the continuum regime. The data in the table are ordered in accordance with the descending pressure drop. The SMF medium has the highest pressure drop and WMF the lowest at all investigated filter face velocities. Furthermore, the average pressure drop gradient across the length of the filter media ($\Delta p_{10^5\,\mathrm{Pa}}$ L^{-1}) is shown in Table 4 to achieve a more accurate understanding of the impact of individual structural parameters (d_p, L, ε) of the pressure drop of the individual filter media.

Table 3
Dimensionless numbers (Re-number, Ma-number and Kn-number) for the flow characterization for the absolute pressure at 10^5 Pa and at 100 Pa for the upstream side (indices i) and the downstream side (indices o) at a filter face velocity of 10 cm s^{-1}.

Absolute pressure	Non-dimensional number	NF	SMF	WMF	SGC	SG
10^5 Pa	Re_i	0.114	0.0133	0.0481	0.0671	0.407
	Re_o	0.1147	0.0141	0.0481	0.068	0.41
	Ma_i	3.55×10^{-4}	4.35×10^{-4}	4.29×10^{-4}	6.2×10^{-4}	6.34×10^{-4}
	Ma_o	3.6×10^{-4}	4.6×10^{-4}	4.3×10^{-4}	6.3×10^{-4}	6.4×10^{-4}
	Kn_i	0.00518	0.055	0.01487	0.015	0.0026
	Kn_o	0.00519	0.058	0.01488	0.016	0.003
100 Pa	Re_i	1.145×10^{-4}	1.328×10^{-5}	4.811×10^{-5}	6.71×10^{-5}	4.07×10^{-4}
	Re_o	1.176×10^{-4}	1.703×10^{-5}	–[a]	1.06×10^{-4}	5.5×10^{-4}
	Ma_i	3.55×10^{-4}	4.35×10^{-4}	4.29×10^{-4}	6.2×10^{-4}	6.34×10^{-4}
	Ma_o	3.7×10^{-4}	5.6×10^{-4}	–[a]	9.8×10^{-4}	8.6×10^{-4}
	Kn_i	5.18	54.65	14.86	15.42	2.6
	Kn_o	5.321	70.116	–[a]	24.391	3.52

[a] Specification not possible as the downstream absolute pressure p_o cannot be reliably determined from the pressure drop because the differential pressure sensor cannot resolve the very low pressure drop in this case.

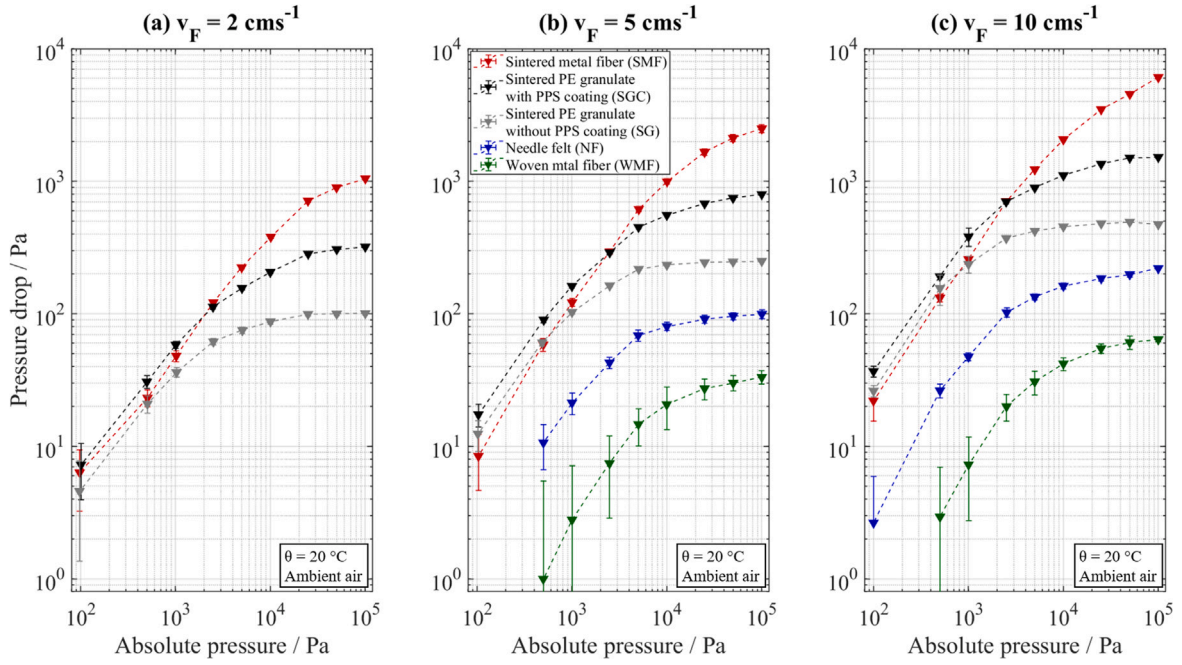

Fig. 6. Variation of the pressure drop as a function of the system pressure for five different filter media at filter face velocities of 2 cm s^{-1}, 5 cm s^{-1} and 10 cm s^{-1}, respectively (at 2 cm s^{-1}, media types NF and WMF were not investigated).

According to the first part (I) of Eq. (3), the pressure drop gradient in the continuum regime is directly proportional to the reciprocal of the square og the pore diameter and the porosity ($\frac{\Delta_p}{L} \sim \frac{1}{d_p^2 \epsilon}$). It can be noted that the mean pore diameter is the dominating factor for the pressure drop gradient when compared to the porosity, due to the fact that the pore diameter enters the equation with a higher power (squared) than the porosity (linear). Additionally, the different filter media exhibit a variation in porosity of less than a factor of 2, whereas the mean pore size varies by a factor of ≈ 20. The pressure drop gradient for individual filter media is observed to increase in accordance with the reduction in mean pore size from the WMF to the SMF medium, with the exception of the SGC medium. Despite the SGC medium having a smaller pore diameter than the WMF medium, it demonstrates a lower pressure drop gradient. This can be attributed to the two-layer structure of the SGC medium: the average pore diameter is primarily indicative of the fine coating, while the thickness is determined by the coarse support layer. Thus, working with global average values for the bi-layered medium results in a misleading low pressure drop gradient when determined by $\Delta p \cdot L^{-}1$

The impact of the thickness of the filter medium is exemplified by the WMF medium. Despite exhibiting the second highest pressure drop gradient, the resulting overall pressure drop is lowest, due to the minimal thickness. The resulting pressure drop is therefore a function of the individual structural parameters and the dominant factor is can be either pore size or media thickness on the specific structural parameters of the medium.

The different mean pore diameters of the filter media result in differing Kn-numbers at a given absolute pressure. Consequently the transition from the slip flow regime to the transition regime occurs at different absolute pressures for the various filter media. This results in an earlier (at higher absolute pressure) steep decline in the pressure drop for the SMF medium. Therefore, the pressure drop curves for the SMF and SGC, as well as for the SMF and SG medium, intersect at a fixed absolute pressure value, regardless of the filter face velocity.

Table 4
Pressure drop at $p_{abs} = 10^5$ Pa ($\Delta p_{10^5\,Pa}$) for all filter face velocities and resulting pressure drop gradient across the filter media.

Filter face velocity	Filter medium	SMF	SGC	SG	NF	WMF
2 cm s^{-1}	$\Delta p_{10^5\,Pa}$/Pa	10.5	3.2	1.0	–[a]	–[a]
	$\Delta p_{10^5\,Pa}$ L^{-1}/Pa m^{-1}	23 300	800	252	–[a]	–[a]
5 cm s^{-1}	$\Delta p_{10^5\,Pa}$/Pa	25	8	2.5	0.9	0.3
	$\Delta p_{10^5\,Pa}$ L^{-1}/Pa m^{-1}	55 471	1994	625	995	4757
10 cm s^{-1}	$\Delta p_{10^5\,Pa}$/Pa	60.9	15.2	4.7	2.2	0.6
	$\Delta p_{10^5\,Pa}$ L^{-1}/Pa m^{-1}	135 311	3798	1181	2201	9157

[a] Measurement not carried out due to the very low resulting pressure drops.

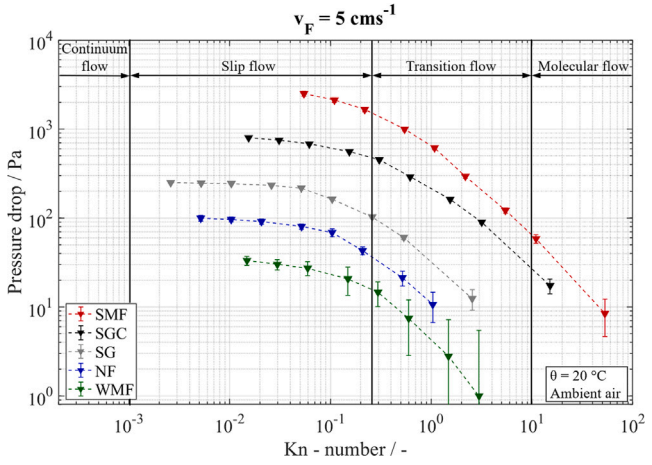

Fig. 7. Pressure drop as a function of the Kn-number for all filter media used at a filter face velocity of 5 cm s^{-1}.

Furthermore, it can be seen that the pressure drop increases with increasing filter face velocity (at a constant absolute pressure) for each filter medium. A proportional dependence of the pressure drop on the filter face velocity can be recognized for the entire investigated absolute pressure range, as was to be expected from Eq. (3). This behavior of the pressure drop corresponds to that found at ambient conditions.

Fig. 7 shows the variation of pressure drop as a function of the Kn-number for all five filter media at 5 cm s^{-1}. In addition, the corresponding flow regimes are shown. It can be seen that the pressure drop decreases as the Kn-number increases. This behavior was to be expected, as the Kn-number is proportional to p_{abs}^{-1}. It can also be observed that the experiments process conditions result mainly in the slip flow and transition flow regime. Molecular flow is reached for the SMF medium and SGC medium. Even at ambient pressure, the continuum flow regime was not reached for any of the filter materials. In order to perform measurements in the continuum flow regime, it would be necessary to investigate absolute pressures above ambient pressure. However, this is not feasible with the experimental setup currently in use and has no relevance in vacuum filtration applications. Fig. 7 clearly show, that the simple calculation equations for the continuum regime cannot be used to determine the pressure drop at higher Kn-numbers. It is necessary to take the rarefaction effect and the slip effect into account in the calculation according to Section 2.

4.3. Determination of the empirical correction factor α

The following sections will introduce two methods for determining the empirical correction factor α, which is required for calculating the pressure drop according to Eq. (3) and (6). The focus will be on the filter face velocities of 2 cm s^{-1}, 5 cm s^{-1} and 10 cm s^{-1} and the absolute pressure range from 100 – 10^5 Pa. The temperature is assumed to be constant ($\theta = 20$ °C) for all further calculations.

In order to calculate the pressure drop as a function of the absolute pressure, it is first necessary to identify an empirical function for the correction factor α. This is achieved by determining the respective α value for the experimental sampling points with the use of Eq. (7). The filter medium properties outlined in Table 1 were employed for the determination of the α values. Fig. 8 shows the calculated α values for 2 cm s^{-1} as squares, for 5 cm s^{-1} as triangles and for 10 cm s^{-1} as circles for all filter media. Diagram (a) shows the complete analyzed absolute pressure range and diagram (b) shows a detail view of the lower absolute pressures close to vacuum conditions. It can be observed that the α values at a given absolute pressure remain largely unaffected by the differences in filter face velocities. Furthermore, different α values can be identified for each filter medium.

The α values calculated in this study differ greatly from the α value range given by Beskok et al. [14]. According to the definition by Beskok et al. α should tend towards zero as the Kn-number decreases, i.e. the absolute pressure becomes higher and tend towards a constant value as the Kn-number becomes very high, i.e the absolute pressure becomes very low [31]. The different behavior of α observed here can be explained by the fact that α in this work does not only cover the rarefaction of the system, as is the case according to Beskok et al. [31]. Beskok et al. have primarily focused their research on simple pipe and gap structures. In this work, complex structured filter media are investigated. α represents therefore a combination of a rarefaction factor and a structure correction factor, thus, it is reasonable to assume that other courses of α will also be observed. Consequently, it is necessary to determine a separate α for the entire pressure range for the calculation of the pressure drop for each individual filter medium. It would be theoretically possible to divide α into two factors: a rarefaction factor and a structure correction factor, by conducting measurements in the continuum regime. However, as previously stated, even at ambient pressure, none of the filter media tested reach into the continuum flow regime.

A simple function is required to describe the dependence of α on the absolute pressure, so that the pressure drop can then be calculated using Eq. (7). Fig. 8 illustrates a linear correlation between the α values and the absolute pressure. In order to evaluate the efficacy of describing the α values as a function of absolute pressure through linear regression, Table 5 presents the coefficient of determination (R^2) for the corresponding filter face velocity and filter medium. R^2 consistently exceeds 95% for all filter media and filter face velocities investigated, suggesting that the α functions for each filter face velocity can be accurately described by a linear equation of the form $\alpha = a \cdot p_{abs} + b$. This linear function of α in dependence of absolute pressure can be described with the use of only two pressure drop measurements and the two corresponding α values. In order to accomplish this, it is recommended that one pressure drop measurement is carried out under ambient conditions and another at a lower absolute pressure.

4.3.1. Determination of the empirical correction factor α with two interpolation points

The process of measuring pressure drop values over a wide range of absolute pressures and filter face velocities for each filter medium is time-consuming and technically much more demanding than a simple air permeability test at ambient pressure. However, as the empirical correction factor α shows an approximately linear curve (Fig. 8 and 5), only two pressure drop measurements are required. Therefore, it is more efficient to only measure the pressure drop for the various filter media and filter face velocities at a specific reduced absolute pressure value and at ambient absolute pressure. In this study, the corresponding pressure drop values at 1000 Pa and 10^5 Pa were used for the estimation of α as a function of the absolute pressure.

The empirical correction factor α calculated at $p_{abs} = 1000$ Pa and 10^5 Pa as a function of the absolute pressure is shown in Fig. 9. The solid line describes the linear fit of α based on the α values at 1000 Pa

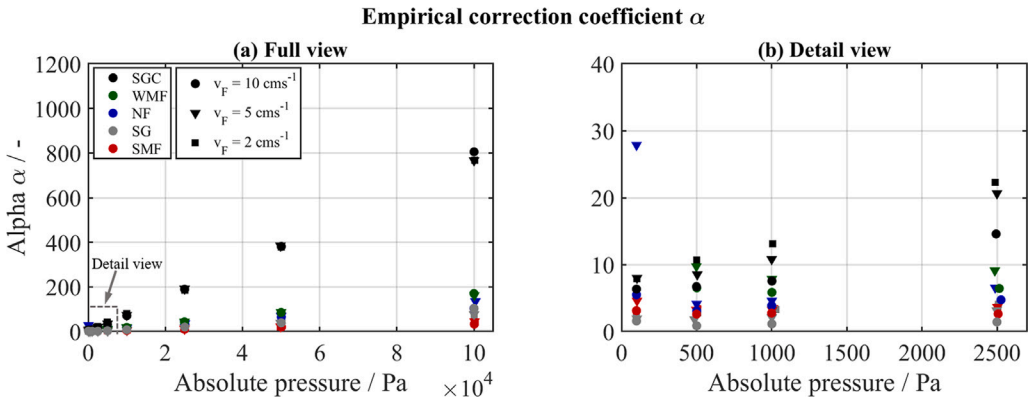

Fig. 8. Empirical correction factor α as a function of absolute pressure for $2\,cm\,s^{-1}$, $5\,cm\,s^{-1}$ and $10\,cm\,s^{-1}$ for all filter media determined with all pressure drop values at ambient temperature and with air. The results are presented in a full view for the complete absolute pressure range (a) and a detail view for the lower end of the absolute pressure range ($\leq 2500\,Pa$) (b).

Table 5
Coefficient of determination for a linear regression of the α values as a function of absolute pressure for the complete range of the analyzed filter face velocities and all filter media.

Filter medium \ Filter face velocity	Coefficient of determination (R^2)		
	$v_F = 2\,cm\,s^{-1}$	$v_F = 5\,cm\,s^{-1}$	$v_F = 10\,cm\,s^{-1}$
SMF	0.9973	0.9948	0.9937
SGC	0.9997	0.9998	0.9995
SG	0.9969	0.9982	0.9950
NF	–[a]	0.9652	0.9867
WMF	–[a]	0.9971	0.9981

[a] Measurement not carried out due to the very low resulting pressure drops.

and 10^5 Pa for $10\,cm\,s^{-1}$, the respective dashed line for $5\,cm\,s^{-1}$ and the dotted line for $2\,cm\,s^{-1}$. Henceforth, this method for calculating α will be referred as Model with two interpolation points (two IP). Again, diagram (a) shows the complete analyzed absolute pressure range and diagram (b) shows a detail view of the lower absolute pressures.

An additional boundary condition was assumed for the fit of the SGC and the SG medium, so that $\alpha(p_{abs} = 100\,Pa) > 0$ remained, as the original regression lines became negative in this area. However, it is not possible to solve Eq. (7) with negative α values.

The α values exhibit minimal discrepancies between the various filter face velocities for all filter media. As the filter face velocity increases, the value of α rises at a constant absolute pressure for all filter media. The SGC medium has the highest α values and also the steepest gradient followed by the WMF medium and the NF medium. The SG medium starts with α values lower than those of the NF medium and higher than those of the SMF medium, but intersects the straight line of the SMF medium at low absolute pressures and thus, a steeper gradient than the SMF medium.

4.3.2. Determination of the empirical correction factor α with one interpolation point and a fixed y-axis value

In most systems for characterizing the pressure drop of surface filter media (e.g. standard procedures according to DIN ISO 11057) or their air permeability (e.g. DIN EN ISO 9237), measurements are only possible under ambient conditions. Thus, a characterization of the pressure drop behavior for a filter medium at low absolute pressure conditions based on the two IP method (see Section 4.3.1) is not feasible. The following section will present a modified method for determining the pressure drop at low pressures, without the requirement for measurements conducted under low absolute pressure conditions.

The detailed view (b) in Fig. 8 of the course of the correction factor α demonstrates that all curves culminate in a comparable y-axis intersection at $p = 0\,Pa$. Accordingly, an average value for each filter face velocity can be calculated from all intercepts of the respective α curves. This yields a value of $\alpha(p = 0\,Pa) = 3$ which can be used as a generic interpolation point without the need for a low absolute pressure measurement. In conjunction with the measurements of the pressure drop at ambient pressure conditions ($p = 10^5$ Pa) at a given temperature and given filter media (Table 2) and fluid specific parameters, a new α can be determined. Just one pressure drop measurement at ambient temperature with air is needed for the calculation of α, so this method will be referred as model with one interpolation point (one IP).

Fig. 10 illustrates the result of a linear fit based on the α values calculated for ambient absolute pressure conditions and ambient temperature and a single fixed y-axis value for all filter media for the complete range of flow velocities. The complete absolute pressure range is illustrated in Diagram (a), while a detail view is presented in Diagram (b).

4.4. Comparison between measured and calculated pressure drop for surface filter media for different filter face velocities

The pressure drop curves calculated using the empirical correction factor α determined with two IP (solid line) and determined with one IP (dashed line) for all tested filter media is presented in Fig. 11. The respective pressure drop curves were calculated with the respective linear α fit function for the specific filter medium at the corresponding filter face velocity. The measured pressure drop values are once more represented as triangles. Diagram (a) illustrates the comparison of the measured and experimental pressure drop at a filter face velocity of $2\,cm\,s^{-1}$, while diagram (b) depicts the same comparison at $5\,cm\,s^{-1}$ and (c) at $10\,cm\,s^{-1}$.

Overall, the calculated pressure drop curves, with the corresponding α fit functions (Model with two IP and Model with one IP), are in good accordance with the measured pressure drop values for all

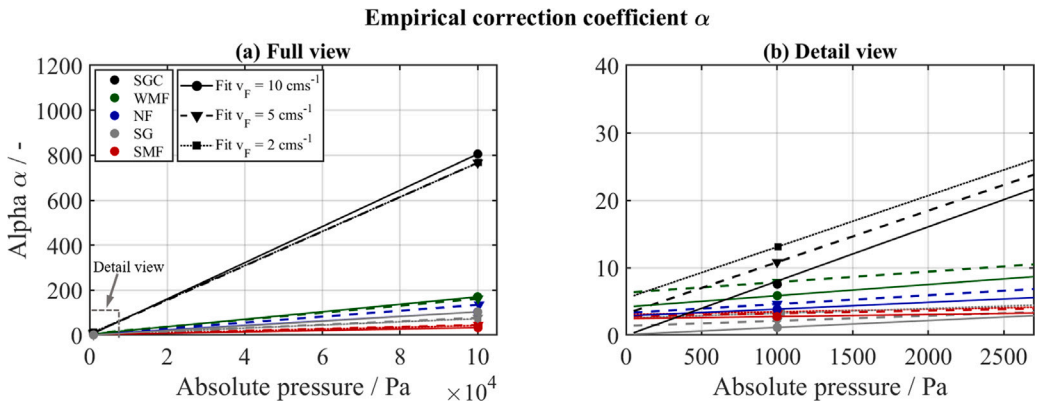

Fig. 9. Empirical correction factor α as a function of absolute pressure for $2\,cm\,s^{-1}$, $5\,cm\,s^{-1}$ and $10\,cm\,s^{-1}$ for all filter media determined with two interpolation points at $p = 1{\times}10^3$ Pa and $p = 10^5$ Pa under ambient temperature and with air. The results are presented in a full view for the complete absolute pressure range (a) and a detail view for the lower end of the absolute pressure range (≤ 2500 Pa) (b).

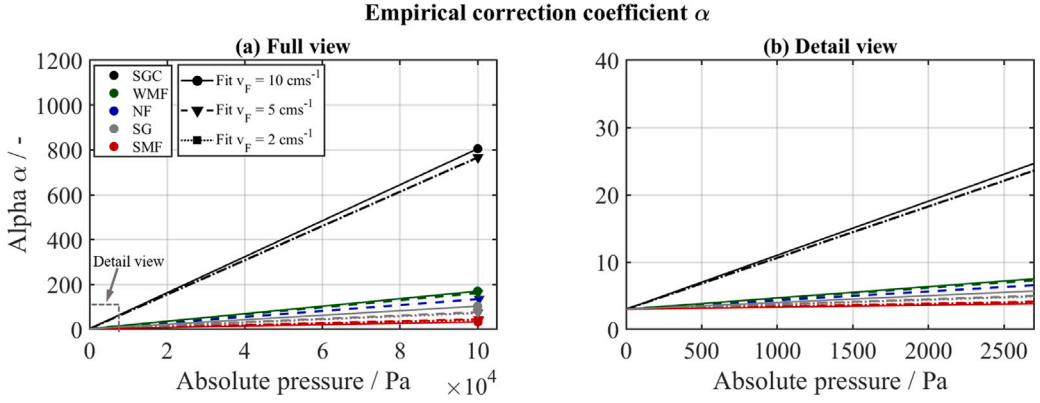

Fig. 10. Empirical correction factor α as a function of absolute pressure for $2\,cm\,s^{-1}$, $5\,cm\,s^{-1}$ and $10\,cm\,s^{-1}$ for all filter media determined with one interpolation point at $p = 10^5$ Pa and a fixed y-axis intercept under ambient temperature and with air. The resulting graph is presented a full view for the complete absolute pressure range (a) and a detail view for the lower end of the absolute pressure range (≤ 2500 Pa) (b).

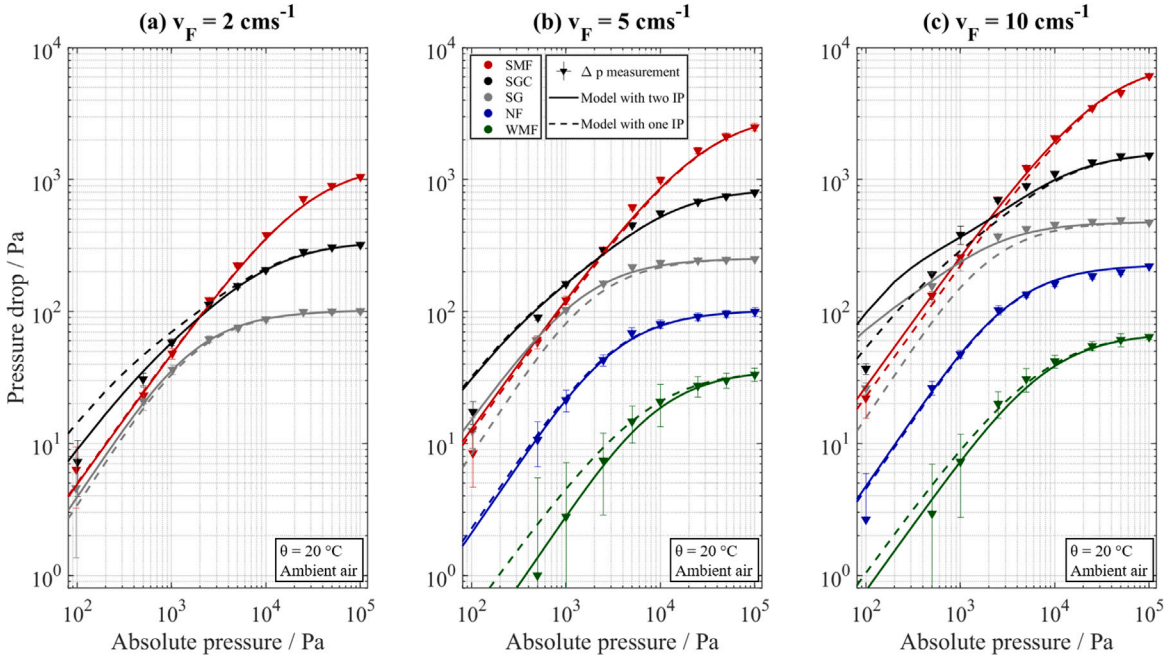

Fig. 11. Comparison of measured pressure drop between the calculated pressure drop with the model that use two IP (solid line) and with the model that use one IP (dashed line) for (a) $2\,cm\,s^{-1}$, (b) $5\,cm\,s^{-1}$ and (c) $10\,cm\,s^{-1}$ for all filter media at ambient temperature with air.

tested filter media at all filter face velocities, especially for higher absolute pressures (max. deviation of 20% for absolute pressures down to 5000 Pa).

For the NF medium, the two variants of calculated pressure drop curves demonstrate a near-identical behavior for all analyzed filter face velocities across the entire absolute pressure range. The generic y-axis interception ($\alpha(p = 0\,Pa) = 3$) is nearly equivalent to the y-axis intersection, which is obtained when a linear regression is conducted using all pressure drop measurements and the corresponding α values from Fig. 8. This explains why the two calculated curves are in close alignment with the measured pressure drop values (max. deviation of 10%). Both pressure drop determination models show nearly the same calculated curves.

Furthermore, the SMF medium shows a high degree of correlation for the two variants of the calculated pressure drop across the entire absolute pressure range, with a slight improvement with reducing the filter face velocity (with a max. deviation of 15% at $2\,cm\,s^{-1}$, a max. deviation of 20% at $5\,cm\,s^{-1}$ and a max. deviation of 24% at $10\,cm\,s^{-1}$). For filter face velocities of $2\,cm\,s^{-1}$ and $5\,cm\,s^{-1}$, the calculated curves for both models are almost identical. However, for a filter face velocity of $10\,cm\,s^{-1}$, there are slight differences between the two curves, which become more pronounced as the absolute pressure decreases.

In case of the WMF medium, the pressure drop curves determined with the α value which was calculated using two IPs exhibit a lower pressure drop level than the model with one IP, within the specified absolute pressure range. The model with two IPs demonstrates a more accurate correlation with the pressure drop measurement data. It is noteworthy that the high relative deviations between the measured and calculated pressure drops (up to 144%) can be identified, particularly for low absolute pressures where the absolute deviations are still small. However, as previously discussed, the accuracy of the measured pressure drop values is limited by the resolution of the differential pressure sensor. In the higher absolute pressure range, the discrepancies between measurement and calculation are also found to be significantly reduced (max. deviation of 26% for $p \geq 2.5 \times 10^3$ Pa for both models).

In the case of the SG medium, a good correlation can be observed between the experimental and theoretical data for both $2\,cm\,s^{-1}$ and $5\,cm\,s^{-1}$ for the model with 2 IP, with a maximum deviation of 22%. At a filter face velocity of $10\,cm\,s^{-1}$, the curve for the model with two IPs is also suitable down to 1000 Pa (maximum deviation 10%), but the discrepancies for low absolute pressures are considerable (maximum deviation of 177%). This can be attributed to the additional boundary condition for the SG medium, which prevents the linear regression of α from assuming negative values (see Section 4.3.1). The accuracy of the model with one IP becomes less precise with increasing filter face velocity for the SG medium (at 2 cm/s, the maximum deviation is 26%, and at 10 cm/s, it is 47%).

For the SGC medium, it should be noted that it is a two-layer filter medium consisting of a thick support structure and a thin coating. The main pressure drop is generated by the thin coating. However, for the calculation of the pressure drop, the total thickness and an average porosity of the complete medium are used, whereas the average pore diameter is related to the coating. These assumptions regarding the structure of the filter medium can lead to issues in calculating the pressure drop. The trends of the calculated pressure drop for the SGC medium are analogous to those for the SG medium. The agreement between the experimental and calculated pressure drop at $2\,cm\,s^{-1}$ is closest, especially for the model with two IP (max deviation of 25%) in the complete absolute pressure range. Both models are almost identical at $5\,cm\,s^{-1}$ and only show a maximum deviation of 14% up to approx. 1000 Pa. For a filter face velocity of $10\,cm\,s^{-1}$, again the additional boundary condition for the fit of α must be considered (see 4.3.1). This results in very high deviations (up to 170%) between the measured and the calculated pressure drop values.

A concise overview of the findings is as follows:

- The discrepancies between the measured and calculated pressure drops increase with increasing filter face velocity
- The relative deviations between the measurement and calculation of the pressure drop values increase with decreasing pressure
- The model with two IP shows better agreement between the experiments and calculation than the model with one IP (exception SG and SGC Medium at $10\,cm\,s^{-1}$)

The presented methodology allows the prediction of the pressure drop behavior for a wide range of surface filter media in the context of rough vacuum conditions. In order to apply the model equations and estimate the pressure drop, it is necessary to have access to the filter media parameters listed in Section 3, as well as at least one pressure drop measurement at a known filter face velocity, temperature and absolute pressure (e.g. ambient pressure). The requisite filter media parameters can often be found in the manufactures data sheet. Furthermore, the air permeability specified in the data sheet can be employed to ascertain the pressure drop at a given filter face velocity. However, the data sheets often provide average values of the air permeability from a large number of different samples of the filter medium. It is notable that surface filter media often display a considerable degree of variation in their structure from one sample to another. Consequently, it is recommended that the pressure drop should be measured under ambient conditions with each individual filter medium sample.

4.4.1. Procedure for calculating the pressure drop of different surface filter media at low absolute pressures

In the following, a procedure is suggested for calculating the pressure drop of different surface filter media at low absolute pressures down to 100 Pa under ambient temperature with air:

1. Measurement of the pressure drop in air under ambient conditions (ambient absolute pressure and temperature) for the filter media to be analyzed at different filter face velocities (recommendation at least two velocities).
2. Calculation of the empirical correction factor α at ambient conditions for the analyzed filter face velocities and filter media applying Eq. (7) using the filter media specific structure parameters (mean porosity, mean pore diameter, thickness) and the fluid specific constants (density and viscosity).
3. Determination of a mean value for each filter medium based on the calculated α values at different filter face velocities. Thus, a single average α value (α_M) is obtained under ambient conditions for each filter medium analyzed.
4. Determine a function for α within the interesting absolute pressure range applying a linear fit between $\alpha(p_{abs} = 100\,Pa) = 3$ and the calculated α values α_M (at $p_{abs} = 10^5$ Pa) for each filter medium.
5. By applying Eq. (7) and the calculated mean α_M curve, the pressure drop as a function of absolute pressure can be determined for each of the analyzed filter media for all filter face velocities of interest.

The result of this procedure for the pressure drop data from this work under ambient temperature and with air is shown in Fig. 12 exemplary for a filter face velocity of $5\,cm\,s^{-1}$ for all filter media used. For absolute pressure ranges exceeding 5×10^3 Pa, the agreement is highly satisfactory, with a maximum deviation of 25% observed across all filter media. As absolute pressure decreases, the relative deviation increases. The NF medium, however, demonstrates a maximum deviation of only 11% across the entire analyzed absolute pressure range.

5. Conclusion and outlook

The objective of this study was to examine the pressure drop behavior of surface filter media under low pressure conditions (rough

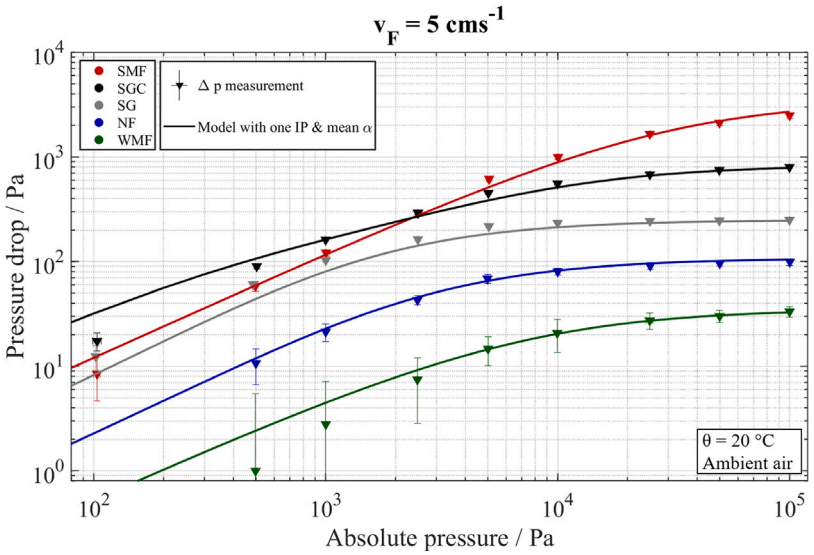

Fig. 12. Comparison of measured pressure drop between calculated pressure drop with the model that use one IP (solid line) determined with a mean α (mean value for $\alpha(p_{abs} = 10^5\,\text{Pa}$ for all three filter face velocities) for all filter media at ambient temperature with air at $5\,\text{cm}\,\text{s}^{-1}$.

vacuum), employing experimental and modeling approaches. To this end, pressure drop measurements were conducted at filter face velocities of $2\,\text{cm}\,\text{s}^{-1}$, $5\,\text{cm}\,\text{s}^{-1}$ and $10\,\text{cm}\,\text{s}^{-1}$ using a low-pressure filtration setup. Five surface filter media, exhibiting significantly different structural properties and surface treatments, were subject to investigation. The absolute pressure in the experimental set up was varied from $p = 100 - 10^5$ Pa. The pressure drop measurements ranged from the slip flow regime to the molecular flow regime.

The measurements demonstrated that the pressure drop decreased at lower absolute pressures. The results are in qualitative agreement with observations reported in literature regarding the pressure drop of depth filter media at low pressures. Furthermore, it was shown that the pressure drop increases to the filter face velocity at a constant reduced absolute pressure, similar to the behavior under ambient pressure.

In order to conduct a theoretical analysis of the pressure drop behavior, a model introduced by Beskok et al. for the flow of fluids through individual long pipes under conditions of a micro- or nano flow was adapted and modified. To apply this model to surface filter media, it is necessary to consider the filter medium structure as an array of straight, parallel pipes. In order to calculate the pressure drop, it is necessary to determine an empirical correction factor α as a function of the absolute pressure. The function $\alpha = f(p_{abs})$ can be derived from a linear fit of individual α values calculated from measured pressure drop values. Two methods were presented for the determination of this linear fit of α as a function of the absolute pressure.

The first method is based on the measurement of two pressure drop values (two IP) at different absolute pressures (one pressure drop measurement at ambient conditions and one at any reduced absolute pressure). While the second method employs the determination of a single pressure drop value (one IP) in conjunction with a fixed generic y-axis interception. Both methods are independent of the filter face velocity. By employing the calculated α curves, in conjunction with the filter media-specific parameters (mean pore size, mean porosity and length) and fluid-specific constants, it is possible to ascertain the pressure drop with the use of Eq. (7). A comparison of the experimental and calculated pressure drop demonstrated a high degree of agreement for all employed filter media. The pressure drop curves derived from the α fit function with two IPs exhibited a greater degree of alignment with the measured pressure drop values than those derived from the α values determined with one IP. The choice between the two calculation methods depends on the desired level of precision in the low absolute pressure range. The method involving two IPs is recommended when a high degree of accuracy is required, whereas the method with one IP is more suitable for applications where a lower level of precision is sufficient.

In addition, a simple calculation procedure for determining the pressure drop at low absolute pressures was presented. In this procedure, a mean α curve was determined based on ambient pressure drop measurements at different filter face velocities and a fixed generic y-axis intercept. This method also shows good agreement between the experimental and calculated pressure drop values for all filter media.

In future work, the formation of filter cakes under low absolute pressures will be examined. It would be of interest to examine whether the model presented in this study for calculating the pressure drop of different unladen surface filter media can also be applied to determine the pressure drop of filter cakes under low pressure conditions. This requires structural properties of the filter cake (such as the filter cake height and the average filter cake porosity). In addition, the influence of low absolute pressure conditions on the size-resolved separation efficiency should be analyzed. To enable these experiments, the experimental setup will be extended to include aerosol generation and aerosol measurement equipment.

CRediT authorship contribution statement

Vanessa Löschner: Methodology, Software, Validation, Formal analysis, Investigation, Data curation, Writing – original draft, Visualization, Project administration. **Jörg Meyer:** Conceptualization, Formal analysis, Writing – review & editing. **Achim Dittler:** Conceptualization, Resources, Writing – review & editing, Supervision, Funding acquisition.

Declaration of competing interest

The authors declare that they have no known competing financial interests or personal relationships that could have appeared to influence the work reported in this paper.

Acknowledgments

We gratefully acknowledge that this project was funded by the Deutsche Forschungsgemeinschaft (DFG, German Research Foundation) – 541566488. We acknowledge the collaboration of Bekaert GmbH for providing the SMF medium, Herding GmbH Filtertechnik for providing

the SG and the SGC medium, Spörl KG for providing the WMF medium and Freudenberg SE for providing the NF medium. Parts of this work were presented at FILTECH 2024.

Data availability

Data will be made available on request.

References

[1] S. Heidenreich, Hot gas filtration – a review, Fuel 104 (2013) 83–94, http://dx.doi.org/10.1016/j.fuel.2012.07.059.
[2] M.W. Jornitz (Ed.), Filtration and purification in the biopharmaceutical industry, third ed., in: Drugs and the pharmaceutical sciences, CRC Press, Taylor & Francis Group, Boca Raton, 2020.
[3] P. Hasler, T. Nussbaumer, Gas cleaning for IC engine applications from fixed bed biomass gasification, Biomass Bioenergy 16 (6) (1999) 385–395, http://dx.doi.org/10.1016/S0961-9534(99)00018-5.
[4] R.C. Brown, Filtration in industrial hygiene, AIHAJ - Am. Ind. Hyg. Assoc. 62 (5) (2001) 633–643, http://dx.doi.org/10.1080/15298660108984663.
[5] T.H. Wines, S. Mokhatab, Contamination Control in the Natural Gas Industry, Gulf Professional Publishing, Cambridge, MA, 2022, OCLC: 1286498889.
[6] C.M. Van'T Land, Drying in the Process Industry, first ed., Wiley, 2011, http://dx.doi.org/10.1002/9781118105818.
[7] W. Jorisch, Vakuumtechnik: in der Chemischen Industrie, Wiley-VCH, Weinheim, 1999, OCLC: 85820458.
[8] B. Thier (Ed.), Apparate Technik - Bau - Anwendung, 2. Ausg, Vulkan-Verl, Essen, 1997, OCLC: 75851114.
[9] F. Löffler, Staubabscheiden, in: Lehrbuchreihe Chemieingenieurwesen/Verfahrenstechnik, vol. 4, Thieme, Stuttgart and New York, 1988.
[10] E. Schmidt, Abscheidung von Partikeln aus Gasen mit Oberflachenfiltern, VDI Verlag, Dusseldorf, 1998, OCLC: 45561735.
[11] P. Li, C. Wang, Y. Zhang, F. Wei, Air filtration in the free molecular flow regime: A review of high-efficiency particulate air filters based on carbon nanotubes, Small 10 (22) (2014) 4543–4561, http://dx.doi.org/10.1002/smll.201401553.
[12] C.N. Davies, Air Filtration, Academic Press, London, New York, 1973.
[13] L. Wu, Rarefied gas dynamics: Kinetic modeling and multi-scale simulation, Springer Nature Singapore, Singapore, 2022, http://dx.doi.org/10.1007/978-981-19-2872-7.
[14] G.E.K. Ali Beskok, Report: A Model for flows in channels, pipes, and ducts at micro and nano scales, Microscale Thermophys. Eng. 3 (1) (1999) 43–77, http://dx.doi.org/10.1080/108939599199864.
[15] D. Richter, Mechanik der Gase, in: Springer-Lehrbuch, Springer Berlin Heidelberg, Berlin, Heidelberg, 2010, http://dx.doi.org/10.1007/978-3-642-12723-6.
[16] J.F. O'Hanlon, A User's Guide to Vacuum Technology, first ed., Wiley, 2003, http://dx.doi.org/10.1002/0471467162.
[17] R.C. Brown, Air Filtration: an Integrated Approach to the Theory and Applications of Fibrous Filters, first ed., Pergamon Press, Oxford ; New York, 1993.
[18] J. Pich, Pressure characteristics of fibrous aerosol filters, J. Colloid Interface Sci. (37) (1971) 912–917.
[19] J. Pich, The drag of a cylinder in the transition region, J. Colloid Interface Sci. 29 (1) (1969) 91–96, http://dx.doi.org/10.1016/0021-9797(69)90350-6.
[20] Z. Liu, D.-R. Chen, P. Wang, Z. Ji, Effect of filtration pressure on the particle penetration efficiency of fibrous filter media, Separ. Purif. Technol. 274 (2021) 119086, http://dx.doi.org/10.1016/j.seppur.2021.119086.
[21] M. He, S. Dhaniyala, M. Wagner, Characterization of filter performance under low-pressure operation, Aerosol Sci. Technol. 50 (5) (2016) 417–428, http://dx.doi.org/10.1080/02786826.2016.1162902.
[22] J.A. Hubbard, J.E. Brockmann, J. Dellinger, D.A. Lucero, A.L. Sanchez, B.L. Servantes, Fibrous filter efficiency and pressure drop in the viscous-inertial transition flow regime, Aerosol Sci. Technol. 46 (2) (2012) 138–147, http://dx.doi.org/10.1080/02786826.2011.616555.
[23] S.C. Stern, H.W. Zeller, A.I. Schekman, The aerosol efficiency and pressure drop of a fibrous filter at reduced pressures, J. Colloid Sci. (15) (1960) 546–562.
[24] N.A. Fuchs, I.B. Stechkina, A note on the theory of fibrous aerosol filters, Ann. Occup. Hyg. 6 (1) (1963) 27–30, Publisher: Oxford University Press.
[25] S. Kuwabara, The forces experienced by randomly distributed parallel circular cylinders or spheres in a viscous flow at small Reynolds numbers, J. Phys. Soc. Japan 14 (4) (1959) 527–532, http://dx.doi.org/10.1143/JPSJ.14.527.
[26] N.A. Fuchs, A.A. Kirsch, I.B. Stechkina, A contribution to the theory of fibrous aerosol filters, Faraday Symp. Chem. Soc. 7 (1973) 143, http://dx.doi.org/10.1039/fs9730700143.
[27] M. Robinson, H. Franklin, The pressure drop of a fibrous filter at reduced ambient pressures, J. Aerosol Sci. 3 (6) (1972) 413–427, http://dx.doi.org/10.1016/0021-8502(72)90072-9.
[28] Y.M. Glushkov, Resistance of fibrous filters in free molecule flow, Fluid Dyn. 3 (4) (1972) 119–122, http://dx.doi.org/10.1007/BF01019213.
[29] J.R. Stalder, G. Goodwin, M.O. Creager, A comparison of theory and experiment for high-speed free-molecule flow, 1950, NTRS Author Affiliations: NTRS Report/Patent Number: NACA-TN-2244 NTRS Document ID: 19930083131 NTRS Research Center: Legacy CDMS (CDMS).
[30] J. Pich, Der Druckabfall der Faserfilter in molekularer Strömung, Staubreinhaltung der Luft 29 (1969) 407–408.
[31] G. Karniadakis, A. Beşkök, N. Aluru, Microflows and nanoflows: fundamentals and simulation, in: Interdisciplinary applied mathematics, (29) Springer, New York, NY, [Heidelberg], 2005.
[32] A. Beskok, Validation of a new velocity-slip model for separated gas microflows, Numer. Heat Transfer B 40 (6) (2001) 451–471, http://dx.doi.org/10.1080/104077901753306593.